



PCCP

**A Charge Transfer State Induced by Strong Exciton Coupling  
in a Cofacial  $\pi$ -Oxo-bridged Porphyrin Heterodimer**

Journal:	<i>Physical Chemistry Chemical Physics</i>
Manuscript ID	CP-ART-11-2020-005783.R1
Article Type:	Paper
Date Submitted by the Author:	09-Dec-2020
Complete List of Authors:	Zarrabi, Niloofar; University of Minnesota Duluth Bayard, Brandon; University of Minnesota Duluth, aDepartment of Chemistry & Biochemistry Seetharaman, Sairaman; University of North Texas Holzer, Noah; University of Minnesota Duluth Karr, Paul; Wayne State College, Department of Physical Sciences and Mathematics Ciuti, Susanna; Università degli Studi di Padova Barbon, Antonio; Università degli Studi di Padova, Dipartimento di Scienze Chimiche di Valentin, Marilena; University of Padova, Chemical Sciences van der Est, Art; Brock University, Chemistry D'Souza, Francis; University of North Texas, Chemistry Poddutoori, Prashanth; University of Minnesota Duluth, Chemistry&Biochemistry

SCHOLARONE™  
Manuscripts

## ARTICLE

# A Charge Transfer State Induced by Strong Exciton Coupling in a Cofacial $\mu$ -Oxo-bridged Porphyrin Heterodimer†

Received 00th January 20xx,  
Accepted 00th January 20xx

DOI: 10.1039/x0xx00000x

Niloofar Zarrabi,<sup>a</sup> Brandon J. Bayard,<sup>a</sup> Sairaman Seetharaman,<sup>b</sup> Noah Holzer,<sup>a</sup> Paul Karr,<sup>c</sup> Susanna Ciuti,<sup>d</sup> Antonio Barbon,<sup>d</sup> Marilena Di Valentin,<sup>d</sup> Art van der Est,<sup>e,\*</sup> Francis D'Souza,<sup>b,\*</sup> Prashanth K. Poddutoorj<sup>a,\*</sup>

Photosensitizers with high energy, long lasting charge-transfer states are important components in systems designed for solar energy conversion by multistep electron transfer. Here, we show that in a push-pull type,  $\mu$ -oxo-bridged porphyrin heterodimer composed of octaethylporphyrinatoaluminum(III) and octaethylporphyrinatosphosphorus(V), the strong excitonic coupling between the porphyrins and the different electron withdrawing abilities of Al(III) and P(V) promote the formation of a high energy CT state. Using, an array of optical and magnetic resonance spectroscopic methods along with theoretical calculations, we demonstrate photodynamics of the heterodimer that involves the initial formation of a singlet CT which relaxes to a triplet CT state with a lifetime of  $\sim$ 130 ps. The high-energy triplet CT state ( ${}^3\text{CT} = 1.68$  eV) lasts for nearly 100  $\mu\text{s}$  prior relaxing to the ground state.

## 1. Introduction

In photosynthesis, light energy from the sun is converted into chemical energy via a series of light reactions in the membrane protein complexes known as reaction centers of photosystems.<sup>1–3</sup> In this intricate process, many optically and redox active molecular components participate to accomplish the energy conversion. The chlorophyll dimer or “special pair” in Photosystem II is of particular interest because it generates an unusually high oxidation potential, which is needed to drive water oxidation.<sup>4–6</sup> The construction of a synthetic analog to the special pair in Photosystem II is an important step to creating artificial photosynthetic devices for the production of clean renewable solar energy. Attempts to create an analog to the special pair have focused on the construction of rigid cofacial porphyrin dimers. These dimers are also of interest for a variety of applications such as model compounds for investigating the dependence of the electronic and optical properties of coupled chromophores as a function of distance and orientation,<sup>7,8</sup> as mimics of photosynthetic energy and electron transfer<sup>9–12</sup> as

catalysts,<sup>13–15</sup> and for host-guest chemistry.<sup>16</sup> Several strategies for their construction have been explored including the use of substituents on the periphery of the porphyrin rings to connect them and hold them in position,<sup>8,17–25</sup> self-assembly in solution by the formation of Lewis acid-base adducts between a substituent on the porphyrin ring and a metal ion center,<sup>16,26,27</sup> and linking the two porphyrins through a  $\mu$ -oxo-bridge between the elements in the centers of the porphyrin rings.<sup>7,15,28–30</sup>

Despite the extensive work on these complexes, relatively little attention has been paid to the physical and spectroscopic properties of cofacial heterodimers in which the two porphyrins can act as electron donor and electron acceptor molecules.<sup>29–33</sup> Within this class of compounds, the  $\mu$ -oxo-heterodimers<sup>29,30</sup> are of particular interest because the porphyrin units are connected via a single oxygen atom axial to both rings. The resulting close proximity causes strong electronic coupling that leads to greater delocalization of the electronic states. If this property is combined with a difference in the redox potentials of the two porphyrins, the lowest excited state of the dimer can be expected to have charge-transfer (CT) character. Such states have been shown to play an important role in initiating high yield light-induced electron transfer in donor-acceptor systems.<sup>34,35</sup> Thus, a porphyrin heterodimer with a CT excited state would be a prime candidate for use as the photosensitizer in photosynthetic reaction center mimics. However, obtaining such a dimer requires fine tuning of the coupling between the porphyrins. If the coupling is too strong, the orbitals become delocalized over the two porphyrins and the difference in their redox potentials is lost. On the other hand, if the coupling is too weak, the excited states become localized and energy transfer can out compete electron transfer. With these considerations in mind, we have investigated the excited state properties of a heterodimer composed of octaethylporphyrinatoaluminum(III)

<sup>a</sup> Department of Chemistry & Biochemistry, University of Minnesota Duluth, 1039 University Drive, Duluth, Minnesota 55812, USA. Email: ppk@d.umn.edu

<sup>b</sup> Department of Chemistry, University of North Texas, 1155 Union Circle, # 305070, Denton, Texas 76203-5017, USA. Email: Francis.Dsouza@UNT.edu

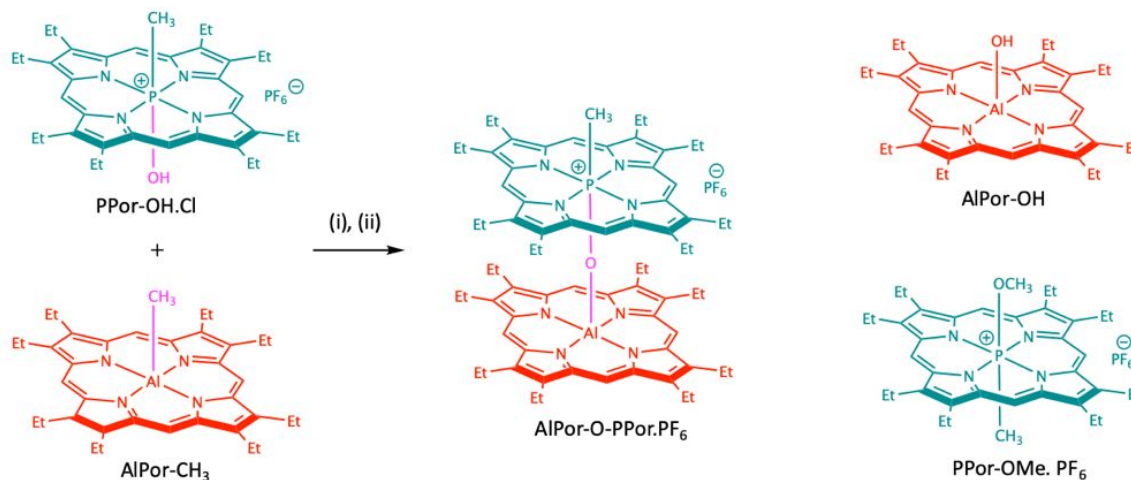
<sup>c</sup> Department of Physical Sciences and Mathematics, Wayne State College, 111 Main Street, Wayne, Nebraska, 68787, USA.

<sup>d</sup> Dipartimento di Scienze Chimiche, Università degli studi di Padova, Via Marzolo 1, 35131 Padova, Italy.

<sup>e</sup> Department of Chemistry, Brock University, 1812 Sir Isaac Brock Way, St. Catharines, ON, L2S 3A1, Canada. Email: avde@brocku.ca

† Electronic Supplementary Information (ESI) available: Details of synthesis and experimental methods, ESI mass spectra, NMR data, absorption data, frontier orbitals of heterodimer, spectral overlaps to calculate  $E_{0,0}$ ,  $E_{\text{CT}}$  and  $E_{\text{T}}$  values, Lippert-Mataga plot, fluorescence spectra, and spectroelectrochemistry of AlPor-OH. See DOI: 10.1039/x0xx00000x

## ARTICLE



**Scheme 1.** Synthesis of heterodimer (AlPor-O-PPor.PF<sub>6</sub>). Reaction conditions: (i) dry toluene, room temperature, stirring under N<sub>2</sub> for 24 h. (ii) NH<sub>4</sub>PF<sub>6</sub>. Structural information of the reference compounds (AlPor-OH, PPor-OMe.PF<sub>6</sub>).

(AlPor) and octaethylporphyrinatophosphorus(V) (PPor<sup>+</sup>) derivatives connected through a  $\mu$ -oxo bridge (see Scheme 1). The synthesis of this compound was first reported by the Akiba group<sup>29,30,36</sup> but its photophysical properties have never been investigated. Because the central atoms Al(III) and P(V) in the porphyrins have different oxidation numbers, the redox potentials of AlPor and PPor<sup>+</sup> differ by about 750 mV. We will show that although some of this difference in redox potential is lost due to the strong interaction between the porphyrins in the  $\mu$ -oxo bridged heterodimer, it remains large enough to generate significant CT character in the lowest excited singlet and triplet states, which are well-poised for secondary electron transfer.

## 2. Experimental section

### 2.1 Synthesis

Scheme 1 shows the synthesis of heterodimer AlPor-O-PPor.PF<sub>6</sub>, see the Supplementary Information for detailed procedures.<sup>30</sup> Compounds AlPor-OH and PPor-OMe.PF<sub>6</sub> (see Scheme 1) were employed as controls in all the spectroscopic and analytical studies. The reference compound PPor-OMe.PF<sub>6</sub> has been reported previously.<sup>37</sup> The compounds AlPor-OH, AlPor-CH<sub>3</sub> and PPor-OH.Cl were synthesized according to the modified procedures, see Supplementary Information of details.

## 3. Results and discussion

### 3.1 Synthesis and characterization

For the synthesis of heterodimer, AlPor-O-PPor.PF<sub>6</sub>, the reactive axial Al—C bond in AlPor-CH<sub>3</sub> was reacted with the acidic hydrogen of the axial hydroxyl of PPor-OH.PF<sub>6</sub>, see Scheme 1. The elimination of methane led to the formation of the heterodimer as a chloride salt in high yields. The resulting compound was found to be very stable under chromatography conditions and after column purification the chloride anion was exchanged for PF<sub>6</sub>. Initial characterization of the heterodimer by ESI high resolution mass spectrometry showed a peak at the expected mass ( $m/z$ ) of [M]<sup>+</sup>, see Fig. S1. The <sup>1</sup>H NMR spectra of AlPor-OH, PPor-OH.PF<sub>6</sub> and AlPor-O-PPor.PF<sub>6</sub> are shown in Figs. S2, S3 and S4, respectively, and the data are summarized in the experimental section. In the porphyrin monomers, AlPor-OH, PPor-OH.PF<sub>6</sub>, the meso-protons of the porphyrin ring appear at 10.31 and 9.61 ppm, respectively. In the heterodimer these protons are shifted to 9.08 and 8.45 ppm, respectively. Similarly, the axial methyl protons of PPor<sup>+</sup>-OH are shifted from  $-5.38$  to  $-7.93$  ppm. The upfield shift of these protons results from the increased shielding from the second porphyrin and confirms the formation of an axially linked cofacial heterodimer with a  $\mu$ -oxo spacer.

### 3.2 UV-visible absorption spectroscopy

The UV-visible spectra of AlPor-O-PPor<sup>+</sup> and its reference compounds (AlPor-OH and PPor<sup>+</sup>-OMe) in CH<sub>2</sub>Cl<sub>2</sub> are shown in Fig. 1. The band positions (Q-band and B- or Soret band) and their molar extinction coefficients are summarized in Table 1. As shown in Fig. 1, the absorption spectrum of the dyad is significantly different from its constituent monomers. The

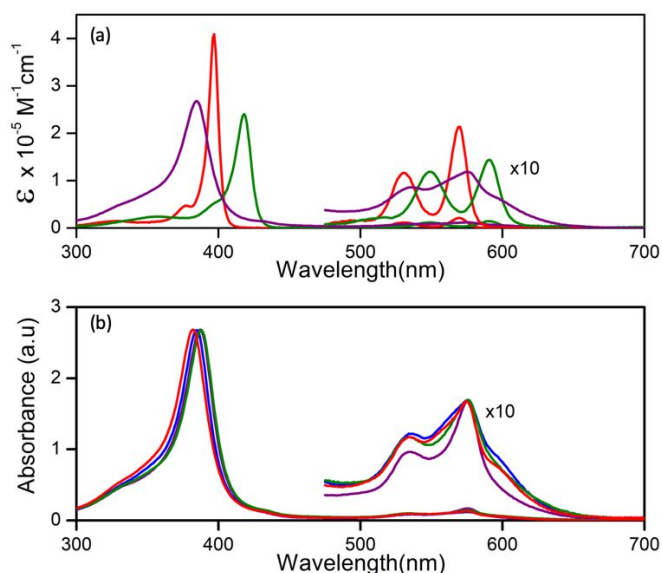


**Fig. 1.** (a) Absorption spectra of AlPor-OH (red), PPor-OMe.PF<sub>6</sub> (green) and AlPor-O-PPor.PF<sub>6</sub> (purple) in CH<sub>2</sub>Cl<sub>2</sub>, and (b) Normalized absorption spectra of AlPor-O-PPor.PF<sub>6</sub> in toluene (purple), CH<sub>2</sub>Cl<sub>2</sub> (blue), o-DCB (green) and CH<sub>3</sub>CN (red).

monomers AlPor and PPor<sup>+</sup> show a sharp Soret band at 397 and 418 nm, respectively. The Soret of the heterodimer is bathochromically shifted to 385 nm and is significantly broader relative to the monomers. Such a shift is expected for a cofacial porphyrin dimer as a result of the excitonic coupling between porphyrin rings. Similar behavior has been observed in various porphyrin dimer systems.<sup>18,20,25</sup> In the Q-band region, PPor<sup>+</sup> has bands at 549 and 591 nm due to Q(1,0) and Q(0,0) transitions.<sup>38</sup> The corresponding AlPor-OH bands occur at 530 and 550 nm. The heterodimer exhibits two Q-bands at 534 and 575 nm and a broad band centered at 600 nm that we assign to the expected charge transfer (CT) absorption. To verify this assignment, the absorption spectra were measured in various solvents (Figs. 1b and S5). As can be seen in the absorption spectra in Fig. 1b, the Soret and Q-bands show a weak solvent dependent shift but no significant change in shape as is expected for excitonically

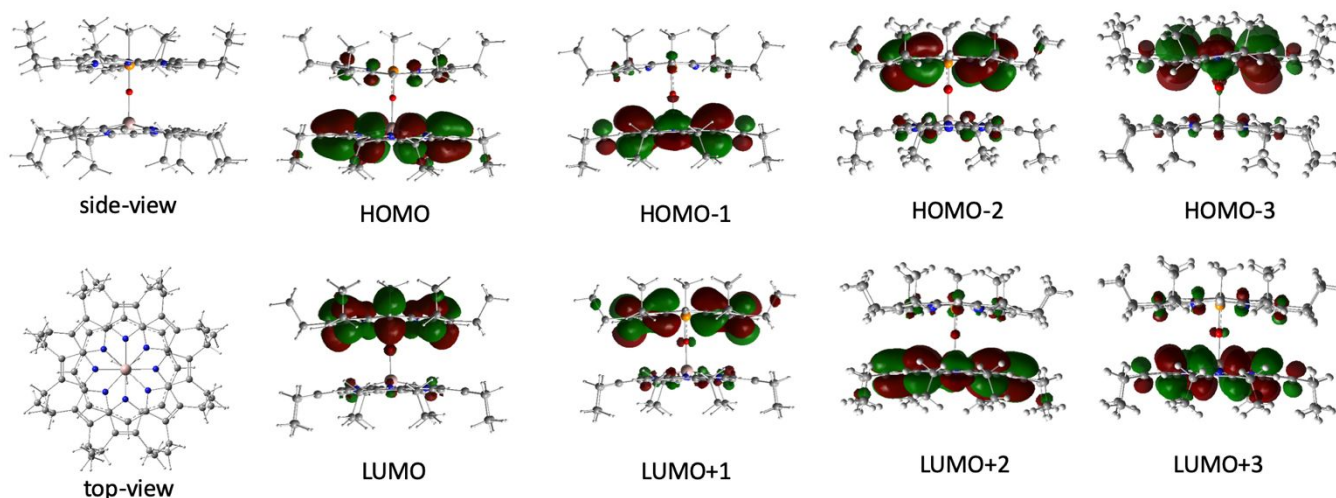
coupled chromophores in dielectric media.<sup>39</sup> In contrast, the intensity of the broad absorption band around 600 nm is higher in polar solvents than in non-polar toluene as is expected for a CT absorption. Such CT bands have also been observed in face-to-face arranged porphyrin-C<sub>60</sub> donor-acceptor systems.<sup>40–45</sup>

### 3.3 DFT calculations

Further, the geometry and electronic structures of the heterodimer were predicted by performing Density Functional Theory (DFT) calculations. Fig. 2 shows optimized structures on a Born-Oppenheimer potential energy surface of the heterodimer calculated using the B3LYP functional and the 6-311G(d, p) basis set as parameterized in Gaussian 16. As shown, the two porphyrin rings are aligned in a face-to-face arrangement with the eight ethyl groups from each porphyrin pointing outside of the heterodimer in a staggered fashion to minimize the steric repulsion; this same phenomenon is also observed in the X-ray crystal structure of the analogous AlPor-O-AsPor<sup>+</sup> dimer.<sup>30</sup> The Al center is slightly above ( $\sim 0.43$  Å) the porphyrin plane. As expected, the HOMO-1 and HOMO are localized predominantly on AlPor whereas the LUMO and LUMO+1 are localized on PPor. However, the most striking observation is a significant delocalization of all the frontier orbitals over both porphyrins (Fig. 2). These observations are very much complementary to the observed absorption results and strongly support the experimental trends. The optimized structures also provide the center-to-center and plane-to-plane distances between AlPor and PPor<sup>+</sup> which are found to be 3.37 and 3.91 Å, respectively.

### 3.4 Cyclic voltammetry and energetics

Cyclic voltammograms of AlPor-O-PPor<sup>+</sup> and the reference compounds were measured in CH<sub>2</sub>Cl<sub>2</sub> with 0.1 M TBA.ClO<sub>4</sub> and ferrocene as an internal standard. Representative voltammograms are shown in Fig. 3, and the data are summarized in Table 1. The redox processes of all of the compounds are found to be one-electron reversible based on

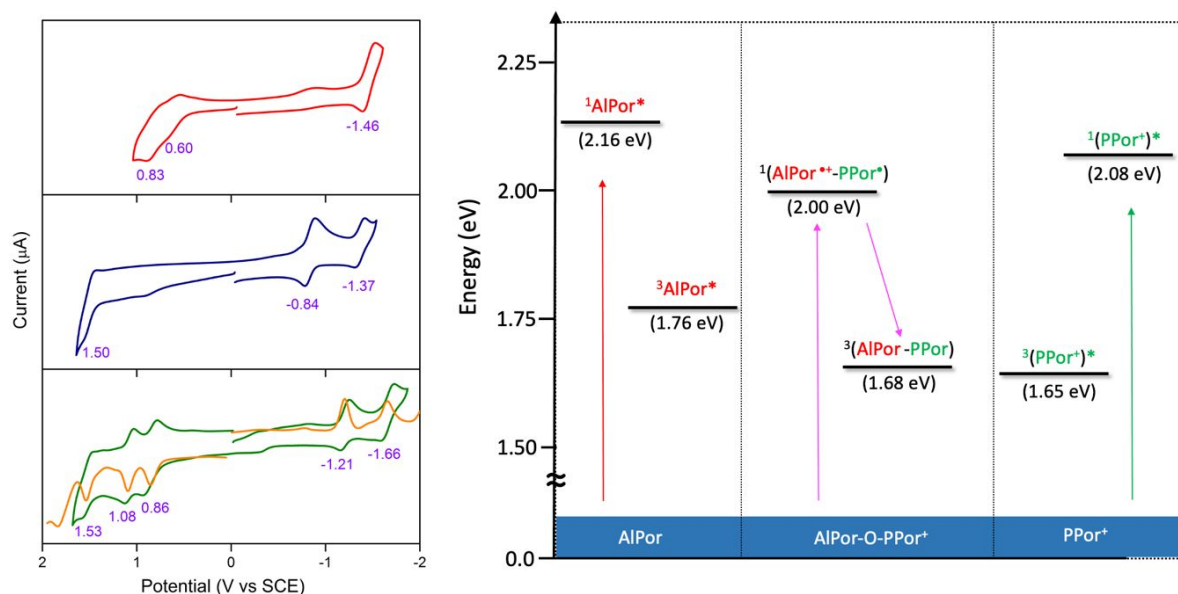


**Fig. 2.** DFT optimized structures and the frontier molecular orbitals of AlPor-O-PPor<sup>+</sup>.

## ARTICLE

**Table 1.** Optical and redox data of investigated compounds in  $\text{CH}_2\text{Cl}_2$ .

Sample	Potential [V vs SCE]		Absorption $\lambda_{\text{max}}$ [nm] ( $\log(\epsilon)$ [ $\text{M}^{-1}\text{cm}^{-1}$ ]))	Fluorescence $\lambda_{\text{max}}$ , nm
	Oxidation	Reduction		
AlPor-OH	0.60, 0.83	-1.46	397 (5.61), 530 (4.07), 550 (4.33)	580, 630
PPor-OMe. $\text{PF}_6$	1.50	-0.84, -1.37	418 (5.38), 549 (4.07), 591 (4.16)	602, 656
AlPor-O-PPor. $\text{PF}_6$	0.86, 1.08, 1.53	-1.21, -1.66	385 (5.43), 534 (3.93), 575 (4.08), 600 (3.76)	574, 598, 668 (broad)

**Fig. 3.** Left: Cyclic voltammogram of AlPor-OH (red), PPor<sup>+</sup>-OMe (blue) and AlPor-O-PPor. $\text{PF}_6$  (green). The differential voltammogram (orange) of AlPor-O-PPor. $\text{PF}_6$  also shown. The experiments performed in  $\text{CH}_2\text{Cl}_2$  with 0.1 M TBA. $\text{ClO}_4$ . Scan rate 100 mV/s. Right: Energy level diagram in  $\text{CH}_2\text{Cl}_2$ .

the peak-to-peak separation values, and the cathodic-to-anodic peak current ratio. The voltammogram of AlPor-OH revealed one reduction at  $-1.46$  V and two oxidation processes at  $0.60$  and  $0.83$  V, whereas the PPor<sup>+</sup>-OMe has one oxidation at  $1.50$  V and two reduction processes at  $-0.84$  and  $-1.37$  V under our experimental conditions. These values clearly show the strong positive shift in potential of PPor<sup>+</sup>-OMe compared to AlPor-OH as a result of the higher oxidation number of P(V) compared to Al(III). The anodic scan of the heterodimer AlPor-O-PPor<sup>+</sup> revealed three oxidation processes at  $0.86$ ,  $1.08$  and  $1.53$  V. The first two of these oxidation potentials correspond to successive removal of electrons from the HOMO, which is localized primarily on AlPor (see Fig. 2). Comparison of the measured values ( $0.86$  and  $1.08$  V) with the corresponding values for

AlPor-OH ( $0.60$  and  $0.83$  V) shows that the delocalization of the HOMO in the heterodimer onto PPor<sup>+</sup> and the presence of the overall positive charge on the heterodimer result in a positive shift of oxidation potentials of about  $+0.25$  V. Formally, the third oxidation should correspond to removal of an electron from the HOMO  $-1$ , which is also mostly localized on AlPor. However, the fact that the oxidation potential ( $+1.53$  V) is the same as the first oxidation of PPor<sup>+</sup> suggests that the electron might come from an orbital that is localized on the PPor<sup>+</sup> half of the heterodimer. The cathodic scan reveals two reduction processes at  $-1.22$  and  $-1.61$  V corresponding the successive addition of two electrons to the LUMO, which is localized primarily on PPor<sup>+</sup>. In this case, delocalization in the heterodimer results in a shift of the potentials by  $-0.38$  and  $-0.24$  V compared those of PPor<sup>+</sup>.

The redox potentials can be used in combination with optical data to construct the energy level diagram of the states involved in possible electron-transfer processes. Fig. 3 summarizes the energy levels of the investigated compounds in  $\text{CH}_2\text{Cl}_2$ . The energies of the lowest excited singlet states ( $E_{0-0}$ ) of AlPor and PPor<sup>+</sup> were calculated from absorption and fluorescence data, Fig. S6. The triplet state energies were obtained from the positions of the phosphorescence bands in the emission spectra as shown in Fig. S6d. The energy of the CT state above the ground state can be roughly estimated using either the difference between first oxidation and reduction potentials of AlPor-O-PPor<sup>+</sup>, the crossing point of the CT absorption and emissive bands or the Rehm-Weller equation,<sup>46</sup> which includes the Coulomb interactions and solvent stabilization. Using the Rehm-Weller equation is problematic in this case because PPor<sup>+</sup> is positively charged and thus electron transfer does not produce two oppositely charged ions. Moreover, the modelling the porphyrins of the dimer as being well-separated spherical ions is not appropriate. The value  $E_{\text{CT}} = 2.07$  eV calculated from the redox potentials is in good agreement with the estimated energy  $E_{\text{CT}} = \sim 2.00$  eV obtained from the crossing point of the absorption and emission bands as shown in Fig. S6c. Thus, we have used the latter value in the energy level diagram in Fig. 3. Regardless of which of these methods is used to estimate the energy of the CT state, they all suggest that the lowest lying excited state of the heterodimer should have considerable charge transfer character. We have tentatively assigned the lowest triplet state of the heterodimer to the CT state on the basis of EPR and transient absorbance data that will be discussed below.

### 3.5. Fluorescence spectroscopy

Steady-state fluorescence spectra of the heterodimer AlPor-O-PPor<sup>+</sup> and its reference compounds AlPor-OH and PPor<sup>+</sup>-OMe were measured in toluene,  $\text{CH}_2\text{Cl}_2$ , *o*-DCB and  $\text{CH}_3\text{CN}$  with

excitation wavelengths of 530 nm, 550 nm, 570 nm and 600 nm. Figs. 4a and 4b show the fluorescence spectra taken in  $\text{CH}_2\text{Cl}_2$  with excitation at 530 and 550 nm, respectively. Corresponding spectra with excitation at 570 and 600 nm are shown in Fig. S7. As can be seen in Figs. 4a and 4b, the reference compounds AlPor and PPor<sup>+</sup> both exhibit two intense relatively narrow emission bands between 550 and 680 nm. In contrast, strong fluorescence quenching occurs in the heterodimer and a shift of the main fluorescence to a broad emission band between 600–800 nm is observed. The fluorescence quenching in the heterodimer indicates the presence of a non-radiative decay pathway that is not present in the monomers. The broad fluorescence band is attributed to emission from the CT state and the low intensity indicates that it has a short lifetime and/or high yield of non-radiative decay. The absence of other fluorescence bands suggests that higher excited states decay via the CT state. Based on the energy level diagram, the driving force for oxidative electron transfer from  $^1\text{AlPor}^*$  to PPor<sup>+</sup> and for reductive electron transfer from AlPor to  $^1(\text{PPor}^+)^*$  is only  $-0.16$  and  $-0.08$  eV, respectively. Despite a small driving force, the heterodimer exhibits strong fluorescence quenching due to strong coupling between the two porphyrin units. The delocalization of the porphyrin frontier orbitals seen in Fig. 2, suggests the excited states involve excitation of both porphyrins and that the lowest excited state has significant CT character. The weak fluorescence intensity suggests that the CT state decays rapidly by either intersystem crossing (ISC) or internal conversion (IC).

### 3.6. Solvatochromism and Lippert-Mataga plot

To further investigate the origin of the broad emission band the solvent dependence of the absorbance and fluorescence was measured. As shown in Fig. 4e, the absorbance spectra are solvent sensitive. In particular, the spectra in THF and  $\text{CH}_3\text{OH}$

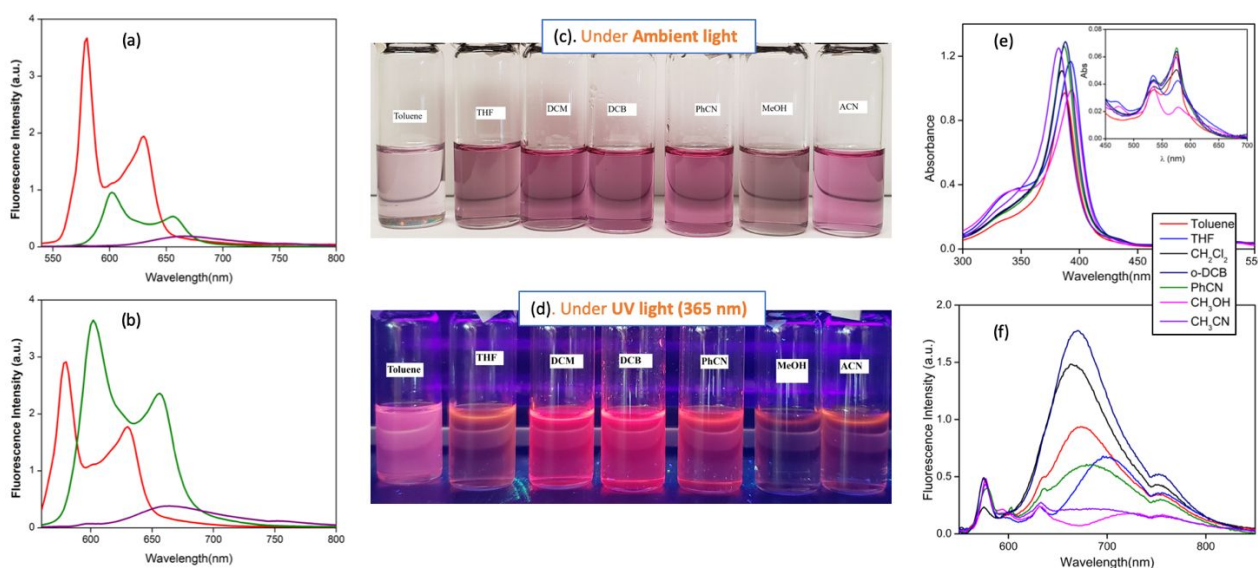


**Fig. 4.** Fluorescence spectra of AlPor-OH (red), PPor-OMe.PF<sub>6</sub> (green) and AlPor-O-PPor.PF<sub>6</sub> (purple) in  $\text{CH}_2\text{Cl}_2$ : (a) excitation at 530 nm and (b) excitation at 550 nm. (c) & (d) Solvatochromism of AlPor-O-PPor.PF<sub>6</sub> in different solvents under (c) ambient light and (d) UV light (365 nm). (e) Absorbance and (f) fluorescence spectra of AlPor-O-PPor.PF<sub>6</sub> in various solvents. Sample concentration =  $1 \times 10^{-6}$  M and excitation wavelength = 530 nm.

## ARTICLE

are very distinctive from other solvents and show new bands at 346 and 475 nm with a decrease in absorbance at 575 nm. These spectral changes are attributed to the enhancement in the exciton coupling between the AlPor and PPor<sup>+</sup> units due to the solvent coordination to the AlPor. Interestingly, these studies also suggest that the nitrogen containing solvents such as CH<sub>3</sub>CN and PhCN, although they are Lewis bases, they are not sufficiently basic enough to coordinate with the Al center of AlPor. However, the absorbance spectra display the CT band as a broad shoulder in all of the investigated solvents, regardless of their Lewis basicity. To visualize the solvatochromism, images of solutions of AlPor-O-PPor<sup>+</sup> taken under ambient light and under UV irradiation (365 nm) are shown in Figs. 4c and 4d. Fig. 4f shows the fluorescence spectra of the heterodimer in various solvents at a concentration of 10<sup>-6</sup> M and excitation at 530 nm. As can be seen in Figs. 4c, d and f, pronounced solvatochromic behavior is observed. Typically, charge-transfer emission shows a bathochromic shift along with a decrease in intensity of emission with increasing solvent polarity.<sup>44,45</sup> This effect is increased in protic solvents when compared to aprotic solvents due to increased secondary interactions such as hydrogen bonding.<sup>47</sup> The origin of the lower CT emission intensity in polar and protic solvents is usually rationalized as a result of weaker mixing of the CT state with higher localized excited states and hence weaker intensity borrowing from the localized excitations.<sup>48</sup> The observed differences in the colors and fluorescence intensities of the samples (Figs. 4c and d) also depends on the emission wavelength. As can be seen in Fig. 4f, the emission band in THF is somewhat outside the visible region and therefore the samples are less colored than those in the other solvents.

The solvent dependence of the Stokes shift of the fluorescence is shown as a Lippert-Mataga plot<sup>49</sup> in Fig. S8 and also provides evidence for charge transfer. As expected for CT fluorescence, the Stokes shift is linearly dependent on the solvent polarity function. Using an Onsager radius of 8 Å for the heterodimer and a dipole moment of 2.82 D for the ground state obtained from DFT calculations, the slope of the Lippert-Mataga plot yields a dipole moment of 11.8 D for the CT state. This value corresponds to a distance of 2.45 Å between two-unit charges, which is in fair agreement with the distance between the porphyrin planes. The scatter in the data in the Lippert-Mataga plot is probably a result of the Lewis acid-base interactions, discussed above, that can occur between solvents such as THF and CH<sub>3</sub>OH and the Al center. The interaction of the complex with the PF<sub>6</sub><sup>-</sup> counterion is also likely to be solvent dependent. All of these factors can be expected to affect the relative energies and mixing of the states of the complex and hence the fluorescence wavelength and intensity. Despite these

complications, the clear solvatochromic effects and linear Lippert-Mataga plot show that the fluorescence arises from the CT state.

### 3.7 Transient absorption spectroscopy

To characterize the formation of the CT state in the heterodimer, femtosecond transient absorption (fs-TA) spectral studies were performed on AlPor-O-PPor<sup>+</sup> and the reference compounds. Fig. 5a shows fs-TA spectra of AlPor-OH in *o*-DCB at the indicated delay times using excitation of the Q-band at 533 nm. The instantaneous formation of <sup>1</sup>AlPor\* results in excited state absorption (ESA) bands at 446, 554, 596, 661 and 1130 nm. In addition, a ground state bleaching (GSB) peak at 532 nm and stimulated emission (SE) peaks at 572 and 631 nm are observed. The 572 nm peak also contains contributions from GSB. The decay/recovery of the positive/negative peaks associated with <sup>1</sup>AlPor\* is longer than the 3 ns time window of the experiment, which is typical for the excited singlet states of porphyrins containing light diamagnetic central elements.<sup>50</sup> At late times, the band around 480 nm and the broad band beyond ~820 nm, probably contain contributions from <sup>3</sup>AlPor\*. The fs-TA data of PPor<sup>+</sup>-OMe (Fig. 5b) show similar behavior. Positive peaks, which we assign to <sup>1</sup>(PPor<sup>+</sup>)\*, are seen at 464, 570, 628 and 1214 nm. The associated GSB and SE peaks are located at 550, 592 and 656 nm. The slow decay/recovery of these positive/negative peaks is consistent with the known excited singlet state lifetime of PPor<sup>+</sup> (5.25 ns for PPor-OMe.PF<sub>6</sub> in CH<sub>3</sub>CN<sup>51</sup>).

As shown in Fig. 5c, the transient absorption spectra of the heterodimer, excited at 533 nm, is distinctly different from either of the monomers. The most obvious of these differences is in the 600–700 nm region where the negative SE band seen in the monomers is absent in the heterodimer spectrum and instead a broad positive ESA band is observed. Using the spectroelectrochemical data for the oxidation of AlPor-OH (Fig. S9) and the reduction of PPor-OMe.PF<sub>6</sub> (reported elsewhere<sup>51</sup>) as a guide, we assign the 600–700 nm ESA band of the heterodimer to the CT state. Other ESA peaks occur at 445 and 552 nm and a broad peak is observed in the 1200–1500 nm region of the near IR that lasts beyond 3 ns delay time. GSB corresponding to the Q-bands also occurs at 535 and 575 nm. The transient spectral data were analyzed further by generating decay associated spectra (DAS) from global analysis of the visible and IR regions, as shown in Figs. 5d and 5e. This analysis resulted in three spectra associated with lifetimes of ~25 ps, ~130 ps and a non-decaying component. In the visible region (Fig. 5d) the DAS of all three components are essentially the same except that the sign of the 26 ps phase is opposite to that of the other two phases. Thus, the 26 ps phase represents the

## ARTICLE

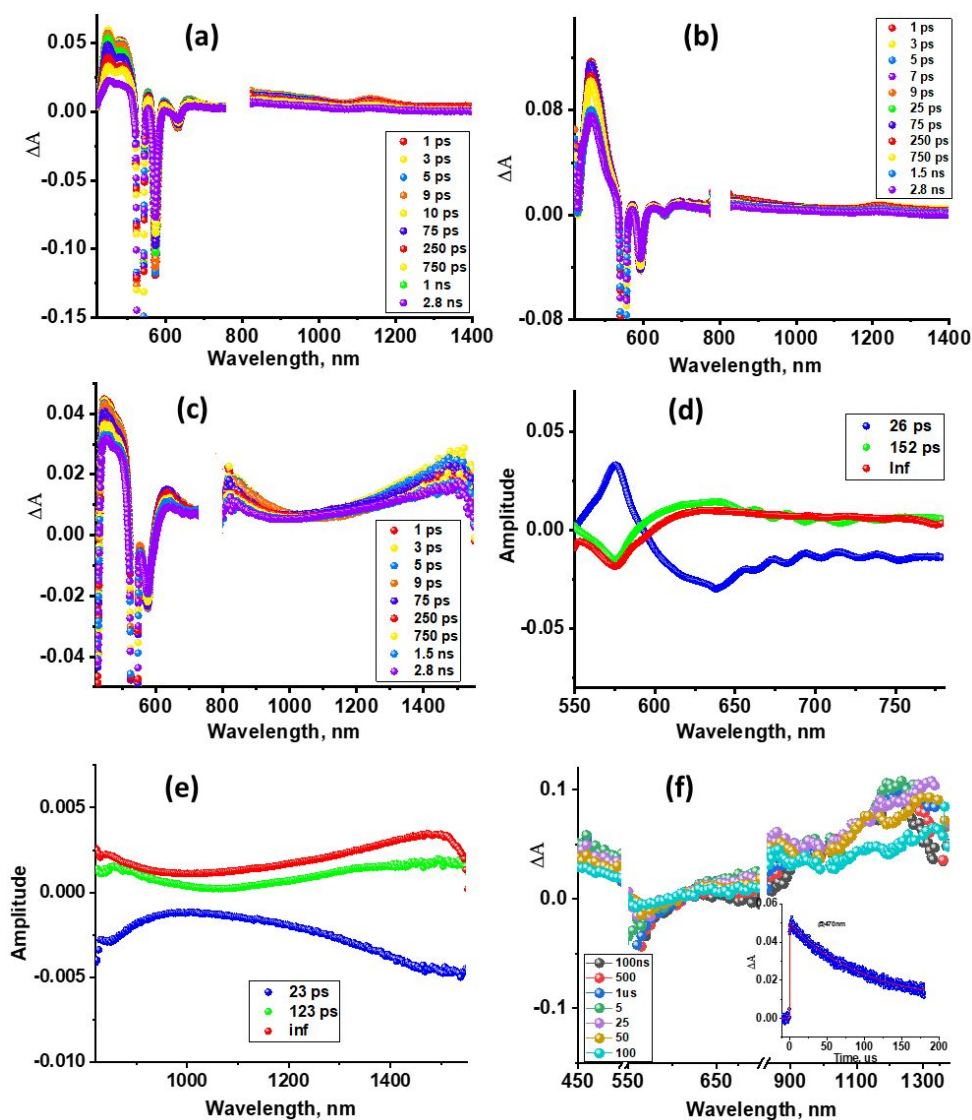


**Fig. 5.** Femtosecond transient absorption spectra of (a) AlPor-OH, (b) PPor-OMe.PF<sub>6</sub>, (c) AlPor-O-PPor-PF<sub>6</sub> heterodimer. (d, e) DAS of spectra of the AlPor-O-PPor-PF<sub>6</sub> heterodimer in the visible region and IR region. (f) Nanosecond transient absorption spectra of the heterodimer in o-DCB at the excitation wavelength of 533 nm. Figure inset shows the decay of 470 nm peak.

rise of the spectrum. Because the GSB rises with this time constant is represents the instrumental response. However, the value of the time constant is longer than the actual instrumental response as the result of inaccuracies in the fitting procedure. The spectra of the 152 ps phase and the non-decaying component both show the broad ESA band between 600-700 nm thus we assign both to the CT state. In the near IR region, the 23 ps phase with negative amplitude represents the rise of the spectrum that decays with 123 ps. However, unlike the visible region, the non-decaying component has a different spectrum

than that of the 123 ps phase with higher amplitude in the 1200-1500 nm range. Thus, we assign the 123 and 152 ps phases to the decay of the CT singlet state and propose that the non-decaying phase corresponds to the CT triplet state.

To gain further support for the existence of the CT triplet state, nanosecond transient absorption spectra (ns-TA) were recorded. The ns-TA spectra of the monomers, AlPor-OH and PPor<sup>+</sup>-OMe is shown in Fig. S10. Both porphyrin derivatives revealed broad peaks in the 450-650 nm range, however, with no noticeable signals in the near-IR region. Decay lifetimes of 86

$\mu\text{s}$  for AlPor-OH and  $99 \mu\text{s}$  for PPor<sup>+</sup>-OMe were obtained. In contrast to these observations, the spectral features of the ns-TA spectra of the AlPor-O-PPor<sup>+</sup>, shown in Fig. 5f, are distinctly different. Peaks at 460, 860 and a broad ESA band in the near-IR region covering the 1100-1350 nm accessible optical window are observed (Fig. 5c). These features largely resemble the non-decaying component obtained from the fs-TA data and are assigned to the triplet CT state. A lifetime of  $105 \mu\text{s}$  for the CT triplet state is obtained from the decay profile shown in the inset to Fig. 5f.

### 3.8 Time-resolved EPR spectroscopy

Since the TA data suggest the formation of a long-lived CT triplet state, we have measured the transient electron paramagnetic resonance (TREPR) spectra of the heterodimer and reference compounds. Fig. 6 shows a comparison of the TREPR spectra of AlPor-OH, PPor<sup>+</sup>-OMe and AlPor-O-PPor<sup>+</sup> measured in a 3:1 mixture of methyl-THF and CH<sub>2</sub>Cl<sub>2</sub> which forms a transparent glass at 80 K. To avoid photoselection effects, the sum of the spectra collected with the laser polarization parallel and perpendicular to the magnetic field is plotted.<sup>52</sup> The spectra of the two monomers (red and green spectra) are typical of porphyrin triplet states and display emission (E) and enhanced absorption (A) as a result of the spin selectivity of spin-orbit coupling mediated intersystem crossing (ISC). The estimated zero-field splitting (ZFS) parameters  $D$  and  $E$  obtained from the spectra are given in Table 2. For planar aromatic compounds that do not contain heavy elements, the spin-orbit coupling contribution to the ZFS is negligible. Thus, the  $D$  and  $E$  values are determined by the spin-spin dipolar interaction and depend on the electron spin distribution. The parameter  $D$  is determined by the average value of the z-component of the interspin vector and the symmetry of the spin distribution. It is largest when the average distance between the spins is small and the spin distribution is highly asymmetric. It is zero for a

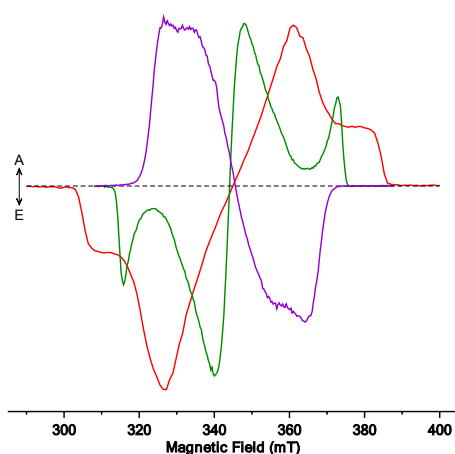


**Fig. 6.** Transient EPR spectra of AlPor-OH (red), PPor<sup>+</sup>-OMe.PF<sub>6</sub> (green) and AlPor-O-PPor<sup>+</sup>.PF<sub>6</sub> (purple). The spectra were extracted from the time/field dataset in a 200 ns wide window centered at 900 ns after laser flash. The samples were measured at 80 K with an excitation wavelength of 575 nm. To avoid photoselection effects the sum  $I_{||} + 2I_{\perp}$  is shown, where  $I_{||}$  and  $I_{\perp}$  are the spectra measured with the polarization of the laser parallel and perpendicular to the magnetic field.<sup>52</sup> Positive features are enhanced absorption (A) and negative features are emission (E).

spherical distribution or infinite distance between the spins. The parameter  $E$  reflects the asymmetry of the ZFS tensor and is zero if the electron spin distribution has 3-fold or higher rotational symmetry. Its maximum value is  $D/3$ . AlPor-OH has approximate  $C_{4v}$  symmetry and as a result the ZFS tensor is nearly axially symmetric i.e.  $E$  is close to zero. Because the two unpaired electrons of the triplet state are distributed over the porphyrin plane,<sup>53</sup> the average value of the z-component of the interspin vector perpendicular to the plane is small and thus, the value of  $D$  is quite large ( $\sim 1$  GHz). The polarization pattern (EEAA) arises from the fact that the x- and y-components of the spin-orbit coupling are larger than the z-component. Thus, the  $m_s$  sublevels of the triplet state are populated according to their x- and y-character.<sup>54</sup> For PPor<sup>+</sup>-OMe, the phosphorus center is much smaller than Al due to its high oxidation number. As a result, the porphyrin ring shows significant deviation from planarity and only has approximate  $C_{2v}$  symmetry. This leads to a reduction in the value of  $D$  and an increase in  $E$  because the symmetry is lower and the difference in the spin distribution in the in-plane and out-of-plane directions becomes smaller.

**Table 2.** Porphyrin zero-field splitting parameters at 80 K.

	$D$ (MHz)	$E$ (MHz)
AlPor-OH	1105	19
PPor <sup>+</sup> -OMe	832	233
AlPor-O-PPor <sup>+</sup>	-650	$\sim 0$

The most noticeable difference between the TREPR spectrum of AlPor-O-PPor<sup>+</sup> and the two porphyrin monomers is the change in sign of the polarization. The spectrum is also narrower than those of the monomers. The change in the sign of the polarization of the triplet spectrum can be due to either a change in the sign of  $D$  or a change in the spin selectivity of the triplet sublevel populations. It is not possible to distinguish between these two possibilities on the basis of the spectrum alone. The energy diagram (Fig. 3) shows that the triplet state of the PPor<sup>+</sup> monomer and the charge transfer triplet state of AlPor-O-PPor<sup>+</sup> have almost the same energy. Thus, in the dimer we can expect there to be two low-lying triplet states one of which has CT character and the other localized primarily on PPor<sup>+</sup>. DFT computations, that will be reported elsewhere, show that the relative energies of these two states depends strongly on how the solvent is modelled. Thus, it is unclear which of the states is lowest in energy under the conditions used for the TREPR experiments. If the charge-transfer triplet state is lowest in energy, the ZFS parameter  $D$  is expected to be negative, while in porphyrin monomers such as AlPor-OH and PPor<sup>+</sup>-OMe, it is known to be positive.<sup>55</sup> The fact that  $E$  is approximately zero (Table 2) is also consistent with greater delocalization of the spins along the z-direction. Using the point-dipole model of two localized electron spins,<sup>56</sup> the observed value of  $D = -650$  MHz in AlPor-O-PPor<sup>+</sup> corresponds to a distance of  $4.9 \text{ \AA}$  between the spins. Although the point-dipole model does not accurately describe the zero-field splitting when the spins are delocalized, the fact that the calculated distance is similar to the interplane distance of  $3.8 \text{ \AA}$  supports the assignment of spectrum to the CT

triplet state. On the other hand, it is also possible that the lowest triplet state is localized mostly on PPor<sup>+</sup>. In this case, the localized triplet state would be populated from either the CT singlet or triplet state and the polarization pattern would depend on the nature of the singlet-triplet mixing in the CT state. Since the CT singlet-triplet energy gap should be comparable to or larger than the Zeeman energy at X-band, net polarization in the spectrum of the localized triplet, i.e. unequal intensity of the absorptive and emissive contributions, is expected. Thus, the narrow width of the spectrum, apparent negative sign of *D*, and the lack of net polarization all suggest that the lowest excited triplet state of the heterodimer has CT character.

#### 4. Conclusions

In conclusion, all of the spectroscopic data point to strong excitonic coupling and the formation of a CT state in the heterodimer. The transient absorbance studies suggest that the CT singlet state decays very rapidly with a lifetime of ~130 ps to the CT triplet state, which has a lifetime of 105 μs. The decay of the TREPR spectrum at 80 K is primarily due to spin relaxation, and shows that the triplet state lifetime is much longer than ~5 μs, in agreement with the TA data. Recently, we showed that rapid intersystem crossing in the photosensitizer can be beneficial in donor-acceptor systems because the long triplet state lifetime allows more time within which the electron transfer can occur.<sup>57–59</sup> This allows the electronic coupling between the photosensitizer and the secondary donor/acceptor to be weaker which in turn helps to stabilize the charge separation. If in addition, the triplet state has significant CT character, as appears to be the case in the heterodimer, it would be ideally poised to promote secondary electron transfer. We are currently exploring this possibility by exploiting the Lewis acidity of the AlPor center to attach a secondary electron donor. The proposed design strategy holds a great promise to mimic the reaction center complex of natural photosynthesis.

#### Conflicts of interest

There are no conflicts to declare.

#### Acknowledgements

This work was supported by Grant-in-Aid (GIA No. 380228 to PPK) from the University of Minnesota Duluth, by the National Science Foundation (Grant No. 2000988 to FD), and by an NSERC Discovery Grant (2015-04021 to AvdE). The computational work was completed utilizing the Holland Computing Center of the University of Nebraska, which receives support from the Nebraska Research Initiative.

#### References

- 1 D. J. Vinyard, G. M. Ananyev and G. Charles Dismukes, Photosystem II: The reaction center of oxygenic photosynthesis, *Annu. Rev. Biochem.*, 2013, **82**, 577–606.
- 2 R. E. Blankenship and H. Hartman, The origin and evolution of oxygenic photosynthesis, *Trends Biochem. Sci.*, 1998, **23**, 94–97.
- 3 R. E. Blankenship, *Molecular Mechanisms of Photosynthesis*, 2008.
- 4 J. Barber, P680: What is it and where is it?, *Bioelectrochemistry*, 2002, **55**, 135–138.
- 5 J. Barber and M. D. Archer, P680, the primary electron donor of photosystem II, *J. Photochem. Photobiol. A Chem.*, 2001, **142**, 97–106.
- 6 J. P. Dekker and R. Van Grondelle, Primary charge separation in Photosystem II, *Photosynth. Res.*, 2000, **63**, 195–208.
- 7 T. Guchhait, S. Sasmal, F. S. T. Khan and S. P. Rath, *Coord. Chem. Rev.*, 2017, **337**, 112–144.
- 8 P. D. Harvey, C. Stern, C. P. Gros and R. Guillard, *Coord. Chem. Rev.*, 2007, **251**, 401–428.
- 9 J. M. Camus, S. M. Aly, D. Fortin, R. Guillard and P. D. Harvey, Design of triads for probing the direct through space energy transfers in closely spaced assemblies, *Inorg. Chem.*, 2013, **52**, 8360–8368.
- 10 J. M. Camus, S. M. Aly, C. Stern, R. Guillard and P. D. Harvey, Acceleration of the through space S1 energy transfer rates in cofacial bisporphyrin bio-inspired models by virtue of substituents effect on the Förster J integral and its implication in the antenna effect in the photosystems, *Chem. Commun.*, 2011, **47**, 8817–8819.
- 11 M. Tanaka, K. Ohkubo, C. P. Gros, R. Guillard and S. Fukuzumi, Persistent electron-transfer state of a π-complex of acridinium ion inserted between porphyrin rings of cofacial bisporphyrins, *J. Am. Chem. Soc.*, 2006, **128**, 14625–14633.
- 12 M. A. Filatov, F. Laquai, D. Fortin, R. Guillard and P. D. Harvey, Strong donor-acceptor couplings in a special pair-antenna model, *Chem. Commun.*, 2010, **46**, 9176–9178.
- 13 E. A. Mohamed, Z. N. Zahran and Y. Naruta, Efficient Heterogeneous CO<sub>2</sub> to CO Conversion with a Phosphonic Acid Fabricated Cofacial Iron Porphyrin Dimer, *Chem. Mater.*, 2017, **29**, 7140–7150.
- 14 P. Peljo, L. Murtomäki, T. Kallio, H. J. Xu, M. Meyer, C. P. Gros, J. M. Barbe, H. H. Girault, K. Laasonen and K. Kontturi, Biomimetic oxygen reduction by cofacial porphyrins at a liquid-liquid Interface, *J. Am. Chem. Soc.*, 2012, **134**, 5974–5984.
- 15 A. B. Sorokin, *Coord. Chem. Rev.*, 2019, **389**, 141–160.
- 16 T. Nakamura, H. Ube and M. Shionoya, Silver-mediated formation of a cofacial porphyrin dimer with the ability to intercalate aromatic molecules, *Angew. Chemie - Int. Ed.*, 2013, **52**, 12096–12100.
- 17 C. Rose, A. Lebrun, S. Clément and S. Richeter, Cofacial porphyrin dimers assembled from N-heterocyclic carbene-metal bonds, *Chem. Commun.*, 2018, **54**, 9603–9606.
- 18 C. A. Hunter, J. K. M. Sanders and A. J. Stone, Exciton coupling in porphyrin dimers, *Chem. Phys.*, 1989, **133**, 395–404.
- 19 M. R. Wasielewski, M. P. Niemczyk and W. A. Svec, Selectively metalated doubly cofacial porphyrin trimers. New models for the study of photoinduced intramolecular electron transfer., *Tetrahedron Lett.*, 1982, **23**, 3215–3218.

- 20 A. Osuka and K. Maruyama, Synthesis of Naphthalene-Bridged Porphyrin Dimers and their Orientation-dependent exciton coupling, *J. Am. Chem. Soc.*, 1988, **110**, 4454–4456.
- 21 I. Fujita, J. Fajer, C. K. Chang, C. B. Wang, M. A. Bergkamp and T. L. Netzel, Solvent and structural effects on picosecond electron transfer reactions in diporphyrin models of the photosystem II reaction center of green plants, *J. Phys. Chem.*, 1982, **86**, 3754–3759.
- 22 L. Moretti, B. Kudisch, Y. Terazono, A. L. Moore, T. A. Moore, D. Gust, G. Cerullo, G. D. Scholes and M. Maiuri, Ultrafast Dynamics of Nonrigid Zinc-Porphyrin Arrays Mimicking the Photosynthetic ‘Special Pair’, *J. Phys. Chem. Lett.*, 2020, **11**, 3443–3450.
- 23 E. A. Mohamed, Z. N. Zahran and Y. Naruta, Covalent bonds immobilization of cofacial Mn porphyrin dimers on an ITO electrode for efficient water oxidation in aqueous solutions, *J. Catal.*, 2017, **352**, 293–299.
- 24 A. Satake, A. Satake, Y. Katagami, Y. Odaka, Y. Kuramochi, Y. Kuramochi, S. Harada, T. Kouchi, H. Kamebuchi, H. Kamebuchi, M. Tadokoro and M. Tadokoro, Synthesis of Double-Bridged Cofacial Nickel Porphyrin Dimers with 2,2'-Bipyridyl Pillars and Their Restricted Coordination Space, *Inorg. Chem.*, 2020, **59**, 8013–8024.
- 25 J. T. Fletcher and M. J. Therien, Extreme electronic modulation of the cofacial porphyrin structural motif, *J. Am. Chem. Soc.*, 2002, **124**, 4298–4311.
- 26 F. D'Souza, R. Chitta, S. Gadde, L. M. Rogers, P. A. Karr, M. E. Zandler, A. S. D. Sandanayaka, Y. Araki and O. Ito, Photosynthetic reaction center mimicry of a ‘special pair’ dimer linked to electron acceptors by a supramolecular approach: Self-assembled cofacial zinc porphyrin dimer complexed with fullerene(s), *Chem. - A Eur. J.*, 2007, **13**, 916–922.
- 27 P. Ballester, M. Claudel, S. Durot, L. Kocher, L. Schoepff and V. Heitz, A Porphyrin Coordination Cage Assembled from Four Silver(I) Triazolyl-Pyridine Complexes, *Chem. - A Eur. J.*, 2015, **21**, 15339–15348.
- 28 L. P. Cailler, M. Clémancey, J. Barilone, P. Maldivi, J. M. Latour and A. B. Sorokin, Comparative Study of the Electronic Structures of  $\mu$ -Oxo,  $\mu$ -Nitrido, and  $\mu$ -Carbido Diiron Octapropylporphyrine Complexes and Their Catalytic Activity in Cyclopropanation of Olefins, *Inorg. Chem.*, 2020, **59**, 1104–1116.
- 29 S. Y. Furuta, M. Yasumoto, Y. Yamamoto and K. Y. Akiba, in *Phosphorus, Sulfur and Silicon and Related Elements*, 2002, vol. 177, pp. 2045–2046.
- 30 G. Yamamoto, R. Nadano, W. Satoh, Y. Yamamoto and K. Y. Akiba, Synthesis of  $\mu$ -oxo-bridged group 15 element-aluminium heterodinuclear porphyrins [(oep)(Me)M-O-Al(oep)]ClO<sub>4</sub> (M = P, As, Sb) and X-ray crystal structure of [(oep)(Me)As-O-Al(oep)]ClO<sub>4</sub>, *Chem. Commun.*, 1997, 1325–1326.
- 31 J. M. Camus, P. D. Harvey and R. Guillard, *Macroheterocycles*, 2013, **6**, 13–22.
- 32 S. Faure, C. Stern, R. Guillard and P. D. Harvey, Role of the Spacer in the Singlet-Singlet Energy Transfer Mechanism (Förster vs Dexter) in Cofacial Bisporphyrins, *J. Am. Chem. Soc.*, 2004, **126**, 1253–1261.
- 33 J. M. Zaleski, C. K. Chang and D. G. Nocera, Influence of solvent dynamics on inverted region electron transfer of cofacial porphyrin-porphyrin and porphyrin-chlorin complexes, *J. Phys. Chem.*, 1993, **97**, 13206–13215.
- 34 S. R. Greenfield, W. A. Svec, D. Gosztola and M. R. Wasielewski, Multistep photochemical charge separation in rod-like molecules based on aromatic imides and diimides, *J. Am. Chem. Soc.*, 1996, **118**, 6767–6777.
- 35 M. R. Wasielewski, Energy, charge, and spin transport in molecules and self-assembled nanostructures inspired by photosynthesis, *J. Org. Chem.*, 2006, **71**, 5051–5066.
- 36 K. Y. Akiba, *Heteroat. Chem.*, 2011, **22**, 207–274.
- 37 P. K. Poddutoori, A. Dion, S. Yang, M. Pilkington, J. D. Wallis and A. Van Der Est, Light-induced hole transfer in a hypervalent phosphorus(V) octaethylporphyrin bearing an axially linked bis(ethylenedithio) tetrathiafulvalene, *J. Porphyr. Phthalocyanines*, 2010, **14**, 178–187.
- 38 P. Sayer, M. Gouterman and C. R. Connell, Porphyrins. 34. Phosphorus Complexes of Octaethylporphyrin, *J. Am. Chem. Soc.*, 1977, **99**, 1082–1087.
- 39 T. Renger and F. Müh, Theory of excitonic couplings in dielectric media : Foundation of Poisson-TrEsp method and application to photosystem I trimers, *Photosynth. Res.*, 2012, **111**, 47–52.
- 40 V. Chukharev, N. V. Tkachenko, A. Efimov and H. Lemmetyinen, Effect of central metal on intra-molecular exciplex of porphyrin-fullerene double linked dyad, *Chem. Phys. Lett.*, 2005, **411**, 501–505.
- 41 F. D'Souza, E. Maligaspe, P. A. Karr, A. L. Schumacher, M. El Ojaimi, C. P. Gros, J. M. Barbe, K. Ohkubo and S. Fukuzumi, Face-to-face pacman-type porphyrin-fullerene dyads: Design, synthesis, charge-transfer interactions, and photophysical studies, *Chem. - A Eur. J.*, 2008, **14**, 674–681.
- 42 D. I. Schuster, P. Cheng, P. D. Jarowski, D. M. Guldi, C. Luo, L. Echegoyen, S. Pyo, A. R. Holzwarth, S. E. Braslavsky, R. M. Williams and G. Klichm, Design, synthesis, and photophysical studies of a porphyrin-fullerene dyad with parachute topology; charge recombination in the marcus inverted region, *J. Am. Chem. Soc.*, 2004, **126**, 7257–7270.
- 43 H. Lehtivuori, H. Lemmetyinen and N. V. Tkachenko, Exciplex-exciplex energy transfer and annihilation in solid films of porphyrin-fullerene dyads, *J. Am. Chem. Soc.*, 2006, **128**, 16036–16037.
- 44 V. Chukharev, N. V. Tkachenko, A. Efimov, D. M. Guldi, A. Hirsch, M. Scheloske and H. Lemmetyinen, Tuning the ground-state and excited-state interchromophore interactions in porphyrin-fullerene  $\pi$ -stacks, *J. Phys. Chem. B*, 2004, **108**, 16377–16385.
- 45 H. Imahori, N. V. Tkachenko, V. Vehmahen, K. Tamaki, H. Lemmetyinen, Y. Sakata and S. Fukuzumi, An extremely small reorganization energy of electron transfer in porphyrin-fullerene dyad, *J. Phys. Chem. A*, 2001, **105**, 1750–1756.
- 46 D. Rehm and A. Weller, Kinetics of Fluorescence Quenching by Electron and H-Atom Transfer, *Isr. J. Chem.*, , DOI:10.1002/ijch.197000029.
- 47 R. Nandy and S. Sankararaman, Donor-acceptor substituted phenylethynyltriphenylenes - Excited state intramolecular charge transfer, solvatochromic absorption and fluorescence emission, *Beilstein J. Org. Chem.*, 2010, **6**, 992–1001.
- 48 M. Bixon, J. Jortner and J. W. Verhoeven, Lifetimes for Radiative Charge Recombination in Donor-Acceptor Molecules, *J. Am.*

- Chem. Soc.*, 1994, **116**, 7349–7355.
- 49 E. Lippert, Dipolmoment und Elektronenstruktur von angeregten Molekülen, *Zeitschrift für Naturforsch. - Sect. A J. Phys. Sci.*, 1955, **10**, 541–545.
- 50 N. Zarrabi, S. Seetharaman, S. Chaudhuri, N. Holzer, V. S. Batista, A. Van Der Est, F. D'Souza and P. K. Poddutoori, Decelerating Charge Recombination Using Fluorinated Porphyrins in N,N-Bis(3,4,5-trimethoxyphenyl)aniline - Aluminum(III) Porphyrin - Fullerene Reaction Center Models, *J. Am. Chem. Soc.*, 2020, **142**, 10008–10024.
- 51 P. K. Poddutoori, G. N. Lim, M. Pilkington, F. D'Souza and A. Van Der Est, Phosphorus(V) Porphyrin-Manganese(II) Terpyridine Conjugates: Synthesis, Spectroscopy, and Photo-Oxidation Studies on a SnO<sub>2</sub> Surface, *Inorg. Chem.*, 2016, **55**, 11383–11395.
- 52 A. Barbon, M. G. Dal Farra, S. Ciuti, M. Albertini, L. Bolzonello, L. Orian and M. Di Valentin, Comprehensive investigation of the triplet state electronic structure of free-base 5,10,15,20-tetrakis(4-sulfonatophenyl)porphyrin by a combined advanced EPR and theoretical approach, *J. Chem. Phys.*, , DOI:10.1063/1.5131753.
- 53 C. W. M. Kay, M. Di Valentin and K. Möbius, A time-resolved Electron Nuclear Double Resonance (ENDOR) study of the photoexcited triplet state of free-base tetraphenylporphyrin, *Sol. Energy Mater. Sol. Cells*, , DOI:10.1016/0927-0248(94)00219-3.
- 54 Y. Hou, X. Zhang, K. Chen, D. Liu, Z. Wang, Q. Liu, J. Zhao and A. Barbon, *J. Mater. Chem. C*, 2019, **7**, 12048–12074.
- 55 S. R. Langhoff, E. R. Davidson, M. Gouterman, W. R. Leenstra and A. L. Kwiram, Zero field splitting of the triplet state of porphyrins. II, *J. Chem. Phys.*, , DOI:10.1063/1.430249.
- 56 Z. Wang, J. Zhao, A. Barbon, A. Toffoletti, Y. Liu, Y. An, L. Xu, A. Karatay, H. G. Yaglioglu, E. A. Yildiz and M. Hayvali, Radical-Enhanced Intersystem Crossing in New Bodipy Derivatives and Application for Efficient Triplet-Triplet Annihilation Upconversion, *J. Am. Chem. Soc.*, 2017, **139**, 7831–7842.
- 57 D. R. Subedi, H. B. Gobeze, Y. E. Kandrashkin, P. K. Poddutoori, A. van der Est and F. D'Souza, Exclusive triplet electron transfer leading to long-lived radical ion-pair formation in an electron rich platinum porphyrin covalently linked to fullerene dyad, *Chem. Commun.*, 2020, **56**, 6058–6061.
- 58 P. K. Poddutoori, Y. E. Kandrashkin, C. O. Obondi, F. D'Souza and A. Van Der Est, Triplet electron transfer and spin polarization in a palladium porphyrin-fullerene conjugate, *Phys. Chem. Chem. Phys.*, 2018, **20**, 28223–28231.
- 59 C. Obondi, G. N. Lim, B. Churchill, P. K. Poddutoori, A. Van Der Est and F. D'Souza, Modulating the generation of long-lived charge separated states exclusively from the triplet excited states in palladium porphyrin-fullerene conjugates, *Nanoscale*, 2016, **8**, 8333–8344.

**TOC Graphic:****A Charge Transfer State Induced by Strong Exciton Coupling in a Cofacial  $\mu$ -Oxo-bridged Porphyrin Heterodimer**

Niloofer Zarrabi, Brandon J. Bayard, Sairaman Seetharaman, Noah Holzer, Paul Karr, Susanna Ciuti, Antonio Barbon, Marilena Di Valentin, Art van der Est, Francis D'Souza, Prashanth K. Poddutoori

